INTERNATIONAL JOURNAL FOR NUMERICAL AND ANALYTICAL METHODS IN GEOMECHANICS
Int. J. Numer. Anal. Meth. Geomech. 2009; **33**:1227–1253
Published online 17 December 2008 in Wiley InterScience (www.interscience.wiley.com). DOI: 10.1002/nag.764

Modeling crack propagation path of anisotropic rocks using boundary element method

Chien-Chung Ke[1,*,†], Chao-Shi Chen[2], Cheng-Yu Ku[3] and Chih-Hao Chen[2]

[1]*Geotechnical Engineering Research Center, Sinotech Engineering Consultants, Inc., Basement No. 7, Lane 26, Yat-Sen Road, Taipei 110, Taiwan*
[2]*Department of Resources Engineering, National Cheng Kung University, Tainan 701, Taiwan*
[3]*Department of Harbor and River Engineering, National Taiwan Ocean University, Keelung 202, Taiwan*

SUMMARY

In a cracked material, the stress intensity factors (SIFs) at the crack tips, which govern the crack propagation and are associated with the strength of the material, are strongly affected by the crack inclination angle and the orientation with respect to the principal direction of anisotropy. In this paper, a formulation of the boundary element method (BEM), based on the relative displacements of the crack tip, is used to determine the mixed-mode SIFs of isotropic and anisotropic rocks. Numerical examples of the application of the formulation for different crack inclination angles, crack lengths, and degree of material anisotropy are presented. Furthermore, the BEM formulation combined with the maximum circumferential stress criterion is adopted to predict the crack initiation angles and simulate the crack propagation paths. The propagation path in cracked straight through Brazilian disc specimen is numerically predicted and the results of numerical and experimental data compared with the actual laboratory observations. Good agreement is found between the two approaches. The proposed BEM formulation is therefore suitable to simulate the process of crack propagation. Copyright © 2008 John Wiley & Sons, Ltd.

Received 14 July 2008; Revised 16 October 2008; Accepted 21 October 2008

KEY WORDS: stress intensity factor; boundary element method; mixed-mode; anisotropic rock; crack propagation path

1. INTRODUCTION

Rock masses in nature contain numerous discontinuities as cracks, joints, cleavages, beddings and/or even faults, etc. Deformation and failure of a rock mass are greatly dependent on the presence of such geological discontinuities. In such a case, the stress intensity factors (SIFs) of

*Correspondence to: Chien-Chung Ke, Geotechnical Engineering Research Center, Sinotech Engineering Consultants, Inc., Basement No. 7, Lane 26, Yat-Sen Road, Taipei 110, Taiwan.
†E-mail: karis.ke@gmail.com, ccke@sinotech.org.tw

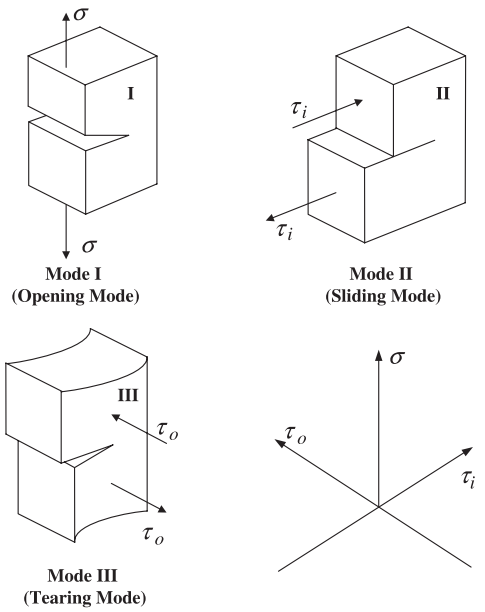

Figure 1. Basic modes of fracture.

crack tips, which govern the crack propagation and are associated with material properties, are strongly affected by the mechanical interaction between cracks.

Fracture mechanics theory has been developed to solve many rock engineering problems, such as cutting, blasting, hydraulic fracturing, and slope stability. The linear elastic fracture mechanics (LEFM) is essentially the extension of Griffith's theory [1] and Irwin's modification [2]. Irwin used SIFs as parameters to describe the stress and the displacement fields near the crack tip. The three SIFs, K_{I}, K_{II} and K_{III}, correspond to three basic fracture modes: mode I, tensile mode (or opening mode), mode II, in-plane shear mode (or sliding mode), and mode III, out-of-plane shear mode (or tearing mode), respectively, as shown in Figure 1. For a given cracked body under a certain type of loading, the SIFs are known and the stresses and displacements near the crack tip can accordingly be determined. Hence, the problem of LEFM reduces to determine the SIFs of the crack tip.

In 2-D crack problems, SIFs are important in analysis of cracked materials. They are directly related to crack propagation criteria. The singularity of stresses near a crack tip is a challenge to numerical modeling methods, even to the BEM. Because the coincidence of the crack surfaces gives rise to a singular system of algebraic equations, the solution of cracked problem cannot be obtained with the direct formulation of the BEM except for Denda [3], who used a physical interpretation of Somigliana's identity to formulate it for the generalized plane strain problem. Several special methods within the scope of the BEM have been suggested for handling stress singularities, such as Green's function method [4, 5], the sub-regional method [6–8], the displacement discontinuity method (DDM) [9–11].

Green's function method overcomes the crack modeling problem without considering any source point along the crack boundaries. This method has the advantage of avoiding crack surface modeling

DOI: 10.1002/nag

and gives excellent accuracy; it is, however, restricted to very simple crack geometries for which analytical Green's function are available. The sub-regional method has the advantage of modeling cracks with any geometric shape. This method has the disadvantage of dividing the boundaries of origin region into several sub-regions; thus, this method cannot be easily implemented as an automatic procedure in an incremental analysis of crack extension problems. The DDM overcomes the crack modeling difficultly by replacing each pair of coincident source points on crack boundaries by a single source point [12]. Instead of using Green's stresses and displacements from point forces, the DDM uses Green's functions corresponding to point dislocations (i.e. displacement discontinuities). This method is quite suitable for crack problems in infinite domains where there is no-crack boundary.

Recently, several single-domain BEMs have been proposed for the study of cracked media [12–24]. As a consequence, general mixed-mode crack problems can be solved in a single-domain BEM formulation. The single-domain analysis can eliminate remeshing problems, which are typical of the FEM and the sub-regional BEM. The single-domain BEM has received considerable attention and has been found to be a good method for simulating crack propagation processes.

One of the single-domain BEMs is the so-called dual boundary element method (DBEM). The essence of this technique is to apply displacement integral equations at one surface of a crack element and traction integral equation at opposite surface, although the two opposing surfaces occupy practically the same space in the model [25]. The hypersingularity involved in the traction integral is evaluated analytically by assuming a piecewise flat crack path. The term DBEM was first presented in Portela [12] and Poterla *et al*. [15, 16]. Extension of this DBEM formulation to the 2-D anisotropic crack problem was reported in Sollero and Aliabadi [17, 18].

In the DBEM formulation, the displacement on each side of the crack surface is collocated as unknown. Thus, the resulting algebraic equations are doubled along the crack surface, which may be unnecessary for SIF calculation. Therefore, an ideal single-domain BEM formulation would be the one which requires discretization on one side of crack surface only. Such single-domain BEM formulation can be achieved by applying the displacement integral equation to the no-crack boundary only, and the traction integral equation on one side of the crack surface only. Since only one side of the crack surface is collocated, one needs to choose either the relative crack displacement (crack opening displacement (COD)). This new BEM formulation can be applied to the general fracture mechanics analysis in anisotropic media while keeping the single-domain merit. Chen *et al*. [26] used the single-domain BEM with J-integral to determine the pure mode I and pure mode II SIFs for cracked discs of anisotropic rock under diametral loading. The J-integral technique, though more accurate in general, has difficulty in handling the cases with the consideration given to the body force, pressurized crack, and curved crack.

Because of the complex shape and continuously changing path of the propagating crack, the BEM results an efficient tool for the analysis of structures and rocks. An early application of the BEM to crack problem is from Cruse [27], with reported accuracy of around 14% for the evaluation of SIFs. Since then the method has been improved and considered as an efficient and accurate numerical technique for the calculation of SIFs and the analysis of crack propagation in LEFM [21].

The prediction of crack initiation and propagation is important for evaluating the safety limits of cracked structures. In the last four decades since Erdogan and Sih [28] developed the first mixed-mode fracture theory, other theories have been formulated. Until now, about eleven theoretical criteria for crack initiation and propagation under mixed-mode I–II loading have been proposed; they are enumerated by Whittaker *et al*. [29]. These include the maximum circumferential stress

DOI: 10.1002/nag

criterion, energy release rate criteria, strain energy density criteria, and other criteria. Boone *et al.* [30] reviewed various theories of crack propagation along with a brief overview of their applicability to different materials and of methods for numerical implementation. In general, the maximum circumferential stress criterion is more popular because of its simplicity [31, 32]. It predicts well the direction of crack initiation and the path of crack propagation compared with experimental results and has been adopted in this paper [11, 26, 33–37].

In this paper, the single-domain BEM formulation combined with the maximum circumferential stress criterion is adopted to predict the crack initiation angles and to simulate the crack propagation paths. Crack propagation in an anisotropic homogeneous plate under mixed-mode I–II loading is simulated by an incremental crack growth with a piecewise linear discretization. A new computer program, which can automatically generate a new mesh required for analyzing the changing boundary configuration sequentially, has been developed to simulate the fracture propagation process. To demonstrate the proposed BEM procedure for predicting crack propagation in anisotropic materials, the propagation path in a cracked straight through Brazilian disc (CSTBD) is numerically predicted and compared with the actual laboratory observations.

The second section of this paper provides the theoretical background including the anisotropy elasticity, boundary element formulation, SIFs determination and crack propagation simulation process. The third and fourth sections of this paper are concern with the accurate determination of SIFs and simulation of crack propagation path using the BEM. There are some numerical examples to verify the proposed BEM formulation.

2. THEORETICAL BACKGROUND

2.1. Anisotropy elasticity

Consider a 2-D thin plate with linear elastic, homogeneous and transversely isotropic properties, as shown in Figure 2. Let x and y be the global Cartesian coordinate system. A local coordinate system x' and y' is attached to the plane of transverse isotropy with the x'-axis taken normal to the plane and the y'-axis being contained within the plane. The inclination angle ψ is defined as the angle between the plane of transverse isotropy and the x-axis. Assume that the plate is thin, it has a plane of elastic symmetry parallel to its middle plane and is loaded by surface forces that

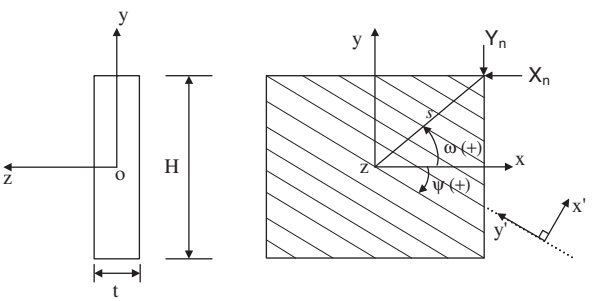

Figure 2. The definition of coordinate system on anisotropic plate.

DOI: 10.1002/nag

vary negligibly across its thickness; therefore, a generalized plane stress formulation can be used [38]. Then, the constitutive relation of the material in the x–y plane can be expressed as

$$\begin{bmatrix} \varepsilon_x \\ \varepsilon_y \\ \gamma_{xy} \end{bmatrix} = \begin{bmatrix} a_{11} & a_{12} & a_{16} \\ a_{21} & a_{22} & a_{26} \\ a_{61} & a_{62} & a_{66} \end{bmatrix} \cdot \begin{bmatrix} \sigma_x \\ \sigma_y \\ \tau_{xy} \end{bmatrix} \tag{1}$$

where $a_{11}, a_{12}, \ldots, a_{66}$ are the compliance components. Using coordinate transformation rules, the a_{ij} can be written in a matrix form as follows [39]:

$$a_{ij} = [D] = [T_\sigma]^{\mathrm{T}} [D'] [T_\sigma] \tag{2}$$

where $[T_\sigma]$ is the second-order tensor transformation and $[D']$ is the elastic constants matrix for transversely isotropic material.

$$[T_\sigma] = \begin{bmatrix} \sin^2\psi & \cos^2\psi & 2\sin\psi\cos\psi \\ \cos^2\psi & \sin^2\psi & -2\sin\psi\cos\psi \\ -\sin\psi\cos\psi & \sin\psi\cos\psi & \sin^2\psi - \cos^2\psi \end{bmatrix}$$

$$[D'] = \begin{bmatrix} 1/E' & -\nu'/E' & 0 \\ -\nu'/E' & 1/E & 0 \\ 0 & 0 & 1/G' \end{bmatrix}$$

where E and E' are Young's modulus in the plane of transverse isotropy and in the direction normal to it, respectively, ν and ν' are Poisson's ratio characterizing the lateral strain response in the plane of transverse isotropy to a stress acting parallel and normal to it, respectively, and G' is the shear modulus in a plane normal to the plane of transverse isotropy.

Let F be a stress function such that

$$\sigma_x = \frac{\partial^2 F}{\partial y^2}, \quad \sigma_y = \frac{\partial^2 F}{\partial x^2}, \quad \tau_{xy} = -\frac{\partial^2 F}{\partial x \partial y} \tag{3}$$

By substituting Equations (1) and (3) into the equation of compatibility, ε_x, ε_y, γ_{xy} must satisfy the following differential equation:

$$a_{22}\frac{\partial^4 F}{\partial x^4} - 2a_{26}\frac{\partial^4 F}{\partial x^3 \partial y} + (2a_{12} + a_{66})\frac{\partial^4 F}{\partial x^2 \partial y^2} - 2a_{16}\frac{\partial^4 F}{\partial x \partial y^3} + a_{11}\frac{\partial^4 F}{\partial y^4} = 0 \tag{4}$$

The general solution of this equation depends on the roots, $\mu_i (i = 1\text{–}4)$ of this characteristic equation,

$$a_{11}\mu^4 - 2a_{16}\mu^3 + (2a_{12} + a_{66})\mu^2 - 2a_{26}\mu + a_{22} = 0 \tag{5}$$

Lekhnitskii [38] showed that the roots of Equation (5) are either complex or purely imaginary, two of them being the conjugate of the other two. Let μ_1, μ_2 be those roots and $\bar{\mu}_1$, $\bar{\mu}_2$ be their respective conjugates. The roots μ_1 and μ_2 are also assumed to be distinct. Substituting Equation (2)

DOI: 10.1002/nag

into Equation (5), it can be shown that for a transversely isotropic plate and for a given inclination angle ψ, the roots depend on E/E', E/G' and ν'. As shown by Lekhnitskii [38], the first derivatives of F with respect to x and y can be expressed as

$$\begin{aligned}\frac{\partial F}{\partial x} &= 2\,\mathrm{Re}[\varphi_1(z_1)+\varphi_2(z_2)]\\ \frac{\partial F}{\partial y} &= 2\,\mathrm{Re}[\mu_1\varphi_1(z_1)+\mu_2\varphi_2(z_2)]\end{aligned} \tag{6}$$

where Re denotes the real part of the complex expression in the brackets and $\varphi_k(z_k)(k=1,2)$ is the analytic function of the complex variables $z_k = x+\mu_k y$.

Combing Equations (3) and (6), we obtain the general expression for the stress components

$$\begin{aligned}\sigma_x &= 2\,\mathrm{Re}[\mu_1^2\varphi_1'(z_1)+\mu_2^2\varphi_2'(z_2)]\\ \sigma_y &= 2\,\mathrm{Re}[\varphi_1'(z_1)+\varphi_2'(z_2)]\\ \tau_{xy} &= -2\,\mathrm{Re}[\mu_1\varphi_1'(z_1)+\mu_2\varphi_2'(z_2)]\end{aligned} \tag{7}$$

where $\varphi_k'(z_k)$ are the first derivatives of $\varphi_k(z_k)$ with respect to z_k. Substituting Equation (7) into the constitutive relation and compatibility equation, the displacement components in the x- and y-directions can be obtained as [40]

$$\begin{aligned}u &= 2\,\mathrm{Re}[P_{11}\varphi_1(z_1)+P_{12}\varphi_2(z_2)]\\ v &= 2\,\mathrm{Re}[P_{21}\varphi_1(z_1)+P_{22}\varphi_2(z_2)]\end{aligned} \tag{8}$$

where

$$\begin{aligned}P_{1k} &= a_{11}\mu_k^2+a_{21}-a_{16}\mu_k\\ P_{2k} &= a_{12}\mu_k+a_{22}/\mu_k-a_{26}\quad (k=1,2)\end{aligned} \tag{9}$$

Considering the concentrated forces acting at the source point (x^0, y^0), the analytic functions (φ_k) with the complex variables can be expressed as [41]

$$\varphi_k(z_k) = \frac{-1}{2\pi}[D_{kl}f_1\ln(z_k-z_k^0)+D_{k2}f_2\ln(z_k-z_k^0)] \tag{10}$$

where $z_k^0 = x^0+\mu_k y^0$ and f_k are the magnitudes of the point force in the k-direction, and

$$\begin{aligned}D_{kl} &= U^{-1}(V^{-1}+\bar{V}^{-1})^{-1}\\ U &= \begin{bmatrix}P_{11} & P_{12}\\ P_{21} & P_{22}\end{bmatrix},\quad V = \mathrm{i}UW^{-1}\\ \mathrm{W} &= \begin{bmatrix}-\mu_1 & -\mu_2\\ 1 & 1\end{bmatrix}\end{aligned} \tag{11}$$

where $\mathrm{i}=\sqrt{-1}$ and overbar means the complex conjugate, superscript -1 means matrix inverse.

DOI: 10.1002/nag

Substituting Equation (10) into Equations (7) and (8), Green's tractions, T_{ij}, and displacements, U_{ij}, (fundamental solutions of this problem) can be expressed as follows [31]:

$$T_{ij}(z_k, z_k^0) = 2\,\mathrm{Re}[Q_{j1}(\mu_1 n_x - n_y)A_{i1}/(z_1 - z_1^0) + Q_{j2}(\mu_2 n_x - n_y)A_{i2}/(z_2 - z_2^0)] \tag{12}$$

$$U_{ij}(z_k, z_k^0) = 2\,\mathrm{Re}[P_{j1}A_{i1}\ln(z_1 - z_1^0) + P_{j2}A_{i2}\ln(z_2 - z_2^0)] \quad (i, j = 1, 2) \tag{13}$$

where n_x and n_y are the outward normal components of the field points and

$$Q_{ij} = -W = \begin{bmatrix} \mu_1 & \mu_2 \\ -1 & -1 \end{bmatrix} \tag{14}$$

The complex coefficients A_{jk} are obtained from the requirements of unit loads at z_k^0 and from the displacement continuity for the fundamental solution. They are the solutions of the following equation:

$$\begin{bmatrix} 1 & -1 & 1 & -1 \\ \mu_1 & -\bar{\mu}_1 & \mu_2 & -\bar{\mu}_2 \\ P_{11} & -\bar{P}_{11} & P_{12} & -\bar{P}_{12} \\ P_{21} & -\bar{P}_{21} & P_{22} & -\bar{P}_{22} \end{bmatrix} \cdot \begin{bmatrix} A_{j1} \\ \bar{A}_{j1} \\ A_{j2} \\ \bar{A}_{j2} \end{bmatrix} = \begin{bmatrix} \delta_{j2}/(2\pi i) \\ -\delta_{j1}/(2\pi i) \\ 0 \\ 0 \end{bmatrix} \tag{15}$$

where δ_{jk} is the Kronecker delta.

2.2. Boundary integral equations

The traditional displacement boundary integral equation for linear elasticity can be expressed as

$$C_{ij}(z_k^0)u_j(z_k^0) + \int_\Gamma T_{ij}(z_k, z_k^0)u_j(z_k)\,\mathrm{d}\Gamma(z_k) = \int_\Gamma U_{ij}(z_k, z_k^0)t_j(z_k)\,\mathrm{d}\Gamma(z_k) \tag{16}$$

where i, j, $k = 1, 2$, T_{ij} and U_{ij} are Green's tractions and displacements given in Equations (12) and (13); u_j and t_j are the boundary displacements and tractions; C_{ij} are quantities that depend on the geometry of the boundary; z_k and z_k^0 are the field and source points on the boundary Γ of the domain. Discretization of Equation (16) gives a linear system of algebraic equations, which can be solved for the unknown displacements u_j and tractions t_j on the boundary. However, for a cracked elastic medium, Equation (16) is not sufficient for solving all the unknowns along the outer boundary of the problem as well as along two sides of the crack surfaces because of the geometric singularity associated with the crack surface.

In the BEM formulation for cracked anisotropic media, the displacement integral equation is collocated on the outer boundary only and the traction integral equation on one side of crack surface only. The displacement integral equation applied to the outer boundary results in the following form ($z_{k,B}^0 \in \Gamma_B$ only, Figure 3):

$$\begin{aligned} &C_{ij}(z_{k,B}^0)u_j(z_{k,B}^0) + \int_{\Gamma_B} T_{ij}(z_{k,B}, z_{k,B}^0)u_j(z_{k,B})\,\mathrm{d}\Gamma(z_{k,B}) \\ &\quad + \int_{\Gamma_C} T_{ij}(z_{k,C}, z_{k,B}^0)[u_j(z_{k,C+}) - u_j(z_{k,C-})]\,\mathrm{d}\Gamma(z_{k,C}) \\ &= \int_{\Gamma_B} U_{ij}(z_{k,B}, z_{k,B}^0)t_j(z_{k,B})\,\mathrm{d}\Gamma(z_{k,B}) \end{aligned} \tag{17}$$

DOI: 10.1002/nag

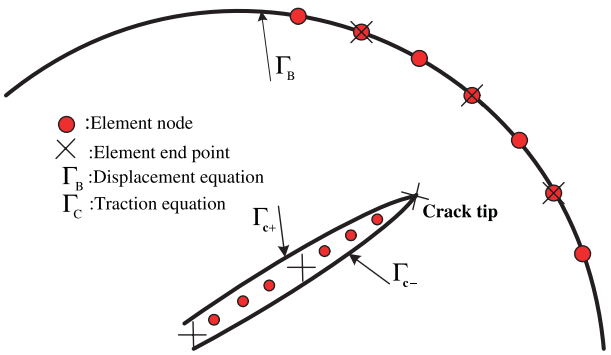

Figure 3. Geometry of a two-dimensional cracked domain.

where Γ_C has the same outward normal as Γ_{C+}. Here, the subscripts B and C denote the outer boundary and the crack surface, respectively.

The traction integral equation (for z_k^0 being a smooth point on the crack) applied to one side of the crack surface is ($z_{k,C}^0 \in \Gamma_{C+}$ only)

$$\begin{aligned} &0.5t_i(z_{k,C}^0) + n_m(z_{k,C}^0)\int_{\Gamma_B} C_{lmik}T_{ij,k}(z_{k,C}^0, z_{k,B})u_j(z_{k,B})\,\mathrm{d}\Gamma(z_{k,B}) \\ &\quad + n_m(z_{k,C}^0)\int_{\Gamma_C} C_{lmik}T_{ij,k}(z_{k,C}^0, z_{k,C})[u_j(z_{k,C+}) - u_j(z_{k,C-})]\,\mathrm{d}\Gamma(z_{k,C}) \\ &= n_m(z_{k,C}^0)\int_{\Gamma_B} C_{lmik}U_{ij,k}(z_{k,C}^0, z_{k,B})t_i(z_{k,B})\,\mathrm{d}\Gamma(z_{k,B}) \end{aligned} \tag{18}$$

where C_{lmik} is the fourth-order stiffness tensor, n_m is the unit outward normal to the contour path, the gradient tensors $T_{ij,k}$ and $U_{ij,k}$ denote differentiation with respect to z_k^0.

The internal stresses $\sigma(z_k)$ are determined by the following expression:

$$\begin{aligned} &\sigma_{lm}(z_k) + \int_{\Gamma_B} C_{lmik}T_{ij,k}(z_{k,C}^0, z_{k,B})u_j(z_{k,B})\,\mathrm{d}\Gamma(z_{k,B}) \\ &\quad + \int_{\Gamma_C} C_{lmik}T_{ij,k}(z_{k,C}^0, z_{k,C})[u_j(z_{k,C+}) - u_j(z_{k,C-})]\,\mathrm{d}\Gamma(z_{k,C}) \\ &= \int_{\Gamma_B} C_{lmik}U_{ij,k}(z_{k,C}^0, z_{k,B})t_j\,\mathrm{d}\Gamma(z_{k,B}) \end{aligned} \tag{19}$$

The Cauchy singularity in Equation (17) can be avoided by the rigid-body motion method. The integrand on the right-hand side of Equation (17) has only integrable singularity, which can be resolved by the bi-cubic transformation method [42]. The hyper-singularity in Equation (18) is resolved by the Gauss quadrature formula, which is very similar to the traditional weighted Gauss quadrature but with a different weight. Therefore, Equations (17) and (18) can be solved simultaneously for the unknown displacements or tractions on the outer boundary and the unknown crack displacement differences on the crack surface.

DOI: 10.1002/nag

2.3. Determination of SIFs

The mixed-mode SIFs for anisotropic media can be determined by using the extrapolation method of the relative COD, combined with a set of the shape functions. The relative COD is defined as [20]

$$\Delta u_i = \sum_{k=1}^{3} \varphi_k \Delta u_i^k \tag{20}$$

where the subscript $i(=1,2)$ denotes the components of the relative COD and the superscript $k(=1,2,3)$ denotes the relative COD at nodes $s=-\frac{2}{3}, 0, \frac{2}{3}$, respectively; φ_k are the shape functions which can be expressed as follows:

$$\begin{aligned}
\varphi_1 &= \tfrac{3\sqrt{3}}{8}\sqrt{s+1}[5-8(s+1)+3(s+1)^2] \\
\varphi_2 &= \tfrac{1}{4}\sqrt{s+1}[-5+18(s+1)-9(s+1)^2] \\
\varphi_3 &= \tfrac{3\sqrt{3}}{8\sqrt{5}}\sqrt{s+1}[1-4(s+1)+3(s+1)^2]
\end{aligned} \tag{21}$$

We assume, for simplicity, that there is a plane of material symmetry normal to the x_3-axis (or x_3-axis is a two-fold symmetry axis). Thus, the displacement u_3 does not couple with the components u_1 and u_2. For this case, the relation of the relative CODs at a distance r behind the crack tip and the SIFs can be found as [7, 20, 40]

$$\begin{aligned}
\Delta u_1 &= 2\sqrt{\frac{2r}{\pi}}(H_{11}K_{\mathrm{I}} + H_{12}K_{\mathrm{II}}) \\
\Delta u_2 &= 2\sqrt{\frac{2r}{\pi}}(H_{21}K_{\mathrm{I}} + H_{22}K_{\mathrm{II}})
\end{aligned} \tag{22}$$

where

$$\begin{aligned}
H_{11} &= \mathrm{Im}\left(\frac{\mu_2 P_{11} - \mu_1 P_{12}}{\mu_1 - \mu_2}\right), \quad H_{12} = \mathrm{Im}\left(\frac{P_{11} - P_{12}}{\mu_1 - \mu_2}\right) \\
H_{21} &= \mathrm{Im}\left(\frac{\mu_2 P_{21} - \mu_1 P_{22}}{\mu_1 - \mu_2}\right), \quad H_{22} = \mathrm{Im}\left(\frac{P_{21} - P_{22}}{\mu_1 - \mu_2}\right)
\end{aligned} \tag{23}$$

Substituting Equation (20) into Equation (22), the SIFs K_{I} and K_{II} can be obtained.

2.4. Crack initiation and propagation

For anisotropic materials, the general form of the elastic stress field near the crack tip in the local Cartesian coordinates x''–y'', as shown in Figure 4, can be expressed in terms of the two SIFs K_{I}

DOI: 10.1002/nag

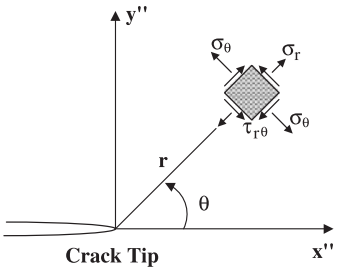

Figure 4. Crack tip coordinate system and stress components.

and K_{II} as follows [43]:

$$\begin{aligned}
\sigma_{x''} &= \frac{K_{\mathrm{I}}}{\sqrt{2\pi r}}\mathrm{Re}\left[\frac{\mu_1\mu_2}{\mu_1-\mu_2}\left(\frac{\mu_2}{\sqrt{\cos\theta+\mu_2\sin\theta}}-\frac{\mu_1}{\sqrt{\cos\theta+\mu_1\sin\theta}}\right)\right] \\
&\quad+\frac{K_{\mathrm{II}}}{\sqrt{2\pi r}}\mathrm{Re}\left[\frac{1}{\mu_1-\mu_2}\left(\frac{\mu_2^2}{\sqrt{\cos\theta+\mu_2\sin\theta}}-\frac{\mu_1^2}{\sqrt{\cos\theta+\mu_1\sin\theta}}\right)\right] \\
\sigma_{y''} &= \frac{K_{\mathrm{I}}}{\sqrt{2\pi r}}\mathrm{Re}\left[\frac{1}{\mu_1-\mu_2}\left(\frac{\mu_1}{\sqrt{\cos\theta+\mu_2\sin\theta}}-\frac{\mu_2}{\sqrt{\cos\theta+\mu_1\sin\theta}}\right)\right] \\
&\quad+\frac{K_{\mathrm{II}}}{\sqrt{2\pi r}}\mathrm{Re}\left[\frac{1}{\mu_1-\mu_2}\left(\frac{1}{\sqrt{\cos\theta+\mu_2\sin\theta}}-\frac{1}{\sqrt{\cos\theta+\mu_1\sin\theta}}\right)\right] \\
\tau_{x''y''} &= \frac{K_{\mathrm{I}}}{\sqrt{2\pi r}}\mathrm{Re}\left[\frac{\mu_1\mu_2}{\mu_1-\mu_2}\left(\frac{1}{\sqrt{\cos\theta+\mu_1\sin\theta}}-\frac{1}{\sqrt{\cos\theta+\mu_2\sin\theta}}\right)\right] \\
&\quad+\frac{K_{\mathrm{II}}}{\sqrt{2\pi r}}\mathrm{Re}\left[\frac{1}{\mu_1-\mu_2}\left(\frac{\mu_1}{\sqrt{\cos\theta+\mu_1\sin\theta}}-\frac{\mu_2}{\sqrt{\cos\theta+\mu_2\sin\theta}}\right)\right]
\end{aligned} \tag{24}$$

where μ_1 and μ_2 are the roots of Equation (5).

$$\sigma_\theta = \frac{\sigma_{x''}+\sigma_{y''}}{2}-\frac{\sigma_{x''}-\sigma_{y''}}{2}\cos 2\theta-\tau_{x''y''}\sin 2\theta \tag{25}$$

$$\tau_{r\theta} = -\frac{\sigma_{x''}-\sigma_{y''}}{2}\sin 2\theta+\sigma_{x''y''}\cos 2\theta \tag{26}$$

For the σ-criterion, the angle of crack initiation, θ_0, must satisfy

$$\frac{\partial\sigma_\theta}{\partial\theta}=0 \text{ (or } \tau_{r\theta}=0) \quad \text{and} \quad \frac{\partial^2\sigma_\theta}{\partial\theta^2}<0 \tag{27}$$

DOI: 10.1002/nag

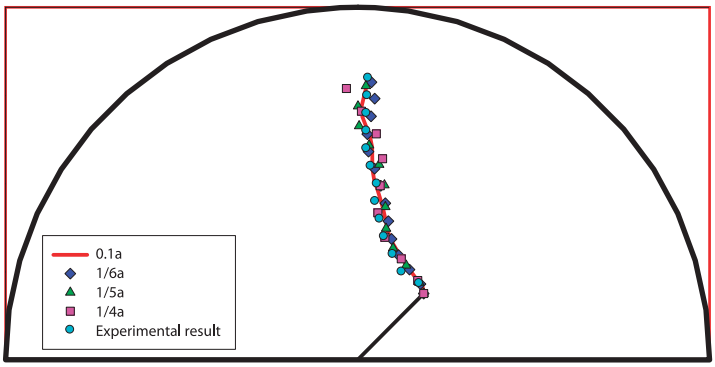

Figure 5. Crack propagation path simulation with different incremental lengths for half-CSTBD specimen ($\psi = 30°, \beta = 45°$).

A numerical procedure is applied to find the angle θ_0 when σ_θ is maximum for known values of the material elastic constants, the anisotropic orientation angle ψ and the crack geometry.

Since the present fracture propagation analysis regards the growth of a single crack, the size of the crack extension incremental can be defined arbitrarily. However, some restrictions on the size are introduced to ensure efficiency of the numerical analysis. For the sake of simplicity, the incremental of the crack extension is discretized with a fixed number of new boundary elements. In order to avoid numerical problems concerned with the relative size of neighboring elements, the size of the crack extension increment is kept constant, between convenient limiting bounds defined in terms of the size of the initial crack tip element [12]. As the crack increment size is related to the accuracy and computational cost of the analysis, there needs to be a balance between the two. Figure 5 shows the variation of crack propagation paths with different incremental lengths for the half-CSTBD specimen ($\psi = 30°, \beta = 45°$) determined numerically and experimentally. A good agreement is found between the experimental results of half-CSTBD specimen and our numerical results with the incremental length of $\frac{1}{6}$ times of the crack tip element. Therefore, the crack increment length is fixed at a size $\frac{1}{6}$ times the crack tip element.

The process of crack propagation in an anisotropic homogeneous material under mixed-mode I–II loading is simulated by incremental crack extension with a piecewise linear discretization. For each incremental analysis, crack extension is conveniently modeled by a new boundary element. A computer program has been developed to automatically generate new data required for analyzing sequentially the changing boundary configuration. Based on the calculation of SIFs and crack initiation angle for each increment, the procedure of crack propagation can be simulated. The steps in the crack propagation process are summarized as follows (Figure 6):

(1) Compute the SIFs using the proposed BEM formulation.
(2) Determine the angle of crack initiation based on the maximum circumferential stress criterion.
(3) Extend the crack by a linear element along the direction determined in step 2.
(4) Automatically generate the new BEM mesh.
(5) Repeat all the above steps until the crack is near the outer boundary.

DOI: 10.1002/nag

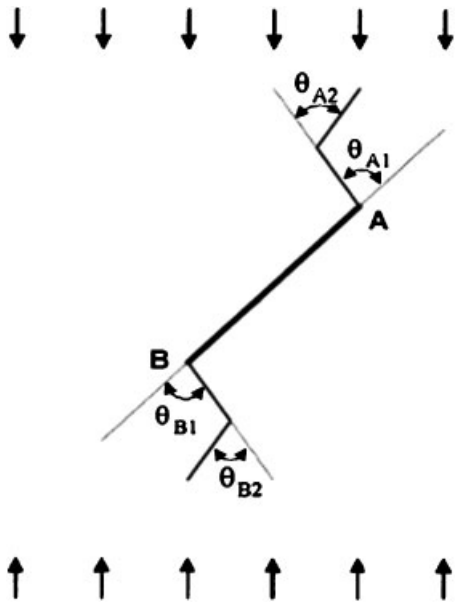

Figure 6. Process of crack propagation by increasing the number of linear elements.

3. ANALYSIS OF SIFs

A computer program, which is based on the aforementioned BEM formulation, has been accomplished to analyze the SIFs for anisotropic materials. The SIFs for both isotropic and anisotropic materials with different crack angles, crack lengths, and anisotropic orientations are analyzed by the program.

Four numerical examples including isotropic and anisotropic materials are presented to illustrate the accuracy and versatility of the proposed BEM program for determining the SIFs. The examples include cases for finite/infinite domains, curved/branched/edge cracks, and isotropic/anisotropic conditions. A generalized plane stress is assumed in all the examples.

Since different element numbers could affect the accuracy of the results of SIFs, the sensitivity analysis is performed to check the appropriate discontinuous element numbers, which are applied to the crack surface. Figure 7 shows the variation of the normalized SIF of mode I with different discontinuous element numbers of crack surface. The numerical results are compared with the analytical solutions obtained by Atkinson *et al*. [44]. We could find that the results between analytical and numerical approaches are very close when using 10 discontinuous quadratic elements. Therefore, 10 or more discontinuous quadratic elements are suitable for determining the SIFs.

Example 1 (*Isotropic cracked Brazilian disc*)
In order to compare our results with the existing published results, an isotropic and cracked Brazilian disc with a central slant crack is considered. The geometry of the problem is that of a thin circular disc of radius R and thickness t with a central crack of length $2a$, loaded with a pair of concentrated and diametral compressive load W, as shown in Figure 8. The outer boundary and crack surface are discretized with 28 continuous and 10 discontinuous quadratic elements,

DOI: 10.1002/nag

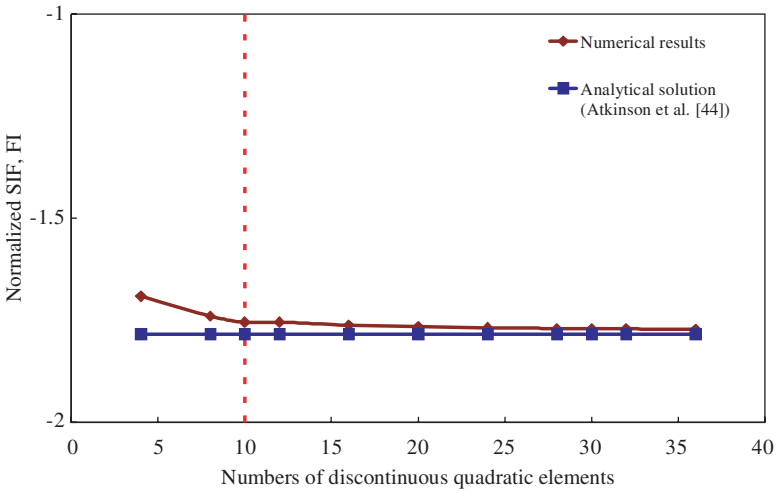

Figure 7. Variation of normalized SIF of mode I with different elements of crack surface.

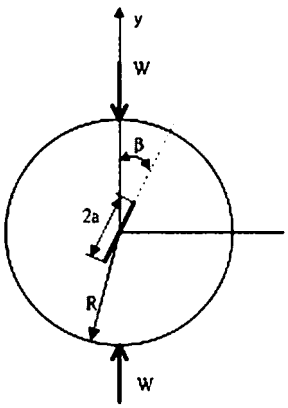

Figure 8. The geometry of cracked Brazilian disc.

respectively. Two cases are analyzed: (1) $a/R=0.5$, the crack angle β varies between 0 and $\pi/2$ and (2) $\beta=45°$, a/R varies between 0.1 and 0.7. The two normalized SIFs, $F_{\mathrm{I}}(=K_{\mathrm{I}}/\sigma\sqrt{\pi a})$ and $F_{\mathrm{II}}(=K_{\mathrm{II}}/\sigma\sqrt{\pi a})$, calculated with the BEM program for these two cases, are compared with those obtained numerically by Atkinson *et al.* [44] and Chen *et al.* [26]. The results are shown in Tables I and II. In general, a good agreement is found among these three methods.

Example 2 (*A curved crack in an infinite domain*)
Consider a circular-arc crack of a radius R embedded in an infinite domain under a far-field tensile stress σ and out-of-plane shear stress τ as shown in Figure 9. The center of the circular arc is taken at the origin of the coordinate system, the midpoint of the crack is located on the x-axis, and the angle subtended by the crack is 2α. In this example only 20 discontinuous quadratic elements are

DOI: 10.1002/nag

Table I. Normalized SIFs for a central slant in an isotropic Brazilian disc subjected to a concentrated load ($a/R=0.5$).

	Atkinson *et al.* [44]		Chen *et al.* [26]		This study	
β (rad)	$K_I/\sigma\sqrt{\pi a}$	$K_{II}/\sigma\sqrt{\pi a}$	$K_I/\sigma\sqrt{\pi a}$	$K_{II}/\sigma\sqrt{\pi a}$	$K_I/\sigma\sqrt{\pi a}$	$K_{II}/\sigma\sqrt{\pi a}$
0	1.387	0	1.339	0	1.343	0
$\pi/16$	0.970	−1.340	0.960	−1.275	0.952	−1.281
$2\pi/16$	0.030	−2.113	0.074	−2.061	0.056	−2.050
$3\pi/16$	−0.946	−2.300	−0.903	−2.275	−0.915	−2.262
$\pi/4$	−1.784	−2.132	−1.737	−2.103	−1.749	−2.098
$5\pi/16$	−2.446	−1.728	−2.377	−1.711	−2.395	−1.714
$6\pi/16$	−2.885	−1.188	−2.826	−1.197	−2.851	−1.202
$7\pi/16$	−3.127	−0.604	−3.092	−0.614	−3.123	−0.617
$\pi/2$	−3.208	0	−3.180	0	−3.213	0

Table II. Normalized SIFs for a central slant in an isotropic Brazilian disc subjected to a concentrated load ($\beta=45°$).

	Atkinson *et al.* [44]		Chen *et al.* [26]		This study	
a/R	$K_I/\sigma\sqrt{\pi a}$	$K_{II}/\sigma\sqrt{\pi a}$	$K_I/\sigma\sqrt{\pi a}$	$K_{II}/\sigma\sqrt{\pi a}$	$K_I/\sigma\sqrt{\pi a}$	$K_{II}/\sigma\sqrt{\pi a}$
0.1	−1.035	−2.010	−1.020	−1.968	−1.018	−1.965
0.2	−1.139	−2.035	−1.116	−1.995	−1.116	−1.992
0.3	−1.306	−2.069	−1.272	−2.036	−1.277	−2.029
0.4	−1.528	−2.100	−1.484	−2.069	−1.492	−2.065
0.5	−1.784	−2.132	−1.737	−2.103	−1.749	−2.098
0.6	−2.048	−2.200	−2.020	−2.148	−2.039	−2.139
0.7	N.A.	N.A.	−2.337	−2.213	−2.364	−2.224

used to discretize the curved crack surface. For $\alpha=30$ and 45°, the numerical solutions of SIFs calculated by this study as well as the analytic ones by Tada *et al.* [45] are shown in Table III.

Example 3 (*Branched crack under a far-field tensile stress and out-of-plane shear stress*)
Figure 10 shows a branched crack under a far-field tensile stress σ and out-of-plane shear stress τ. The main crack has a length a and each branch has a length b, with ratios $b/a=0.6$. The branches are located symmetrically on both sides of the main crack and inclined at $\alpha=45°$ to it. It is noteworthy that at the function of the branch cracks, the relative COD and the integration of the traction should be satisfied, respectively, the continuity and equilibrium conditions derived by Ammons and Vable [46]. However, collocations at the branch point can be avoided using discontinuous element. In this example, 10 discontinuous quadratic elements are used for main crack surface, six elements for each branch when $b/a=0.6$. The numerical results for this example were evaluated in Murakami [47] and were also solved by Ammons and Vable [46]. In Table IV, the normalized SIFs of the crack tips A and B are given for the ratio $b/a=0.6$ and compared with those obtained by Ammons and Vable [46] and Murakami [47].

DOI: 10.1002/nag

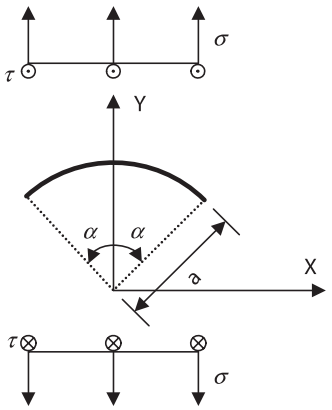

Figure 9. A curved crack under a far-field tensile stress σ and out-of-plane shear stress τ.

Table III. Normalized SIFs for a circular-arc crack in an infinite domain.

	Tada *et al.* [45]		This study	
α	$K_{\mathrm{I}}/\sigma\sqrt{\pi a}$	$K_{\mathrm{II}}/\sigma\sqrt{\pi a}$	$K_{\mathrm{I}}/\sigma\sqrt{\pi a}$	$K_{\mathrm{II}}/\sigma\sqrt{\pi a}$
30°	0.5501	0.3304	0.5528	0.3288
45°	0.4574	0.5112	0.4643	0.5126

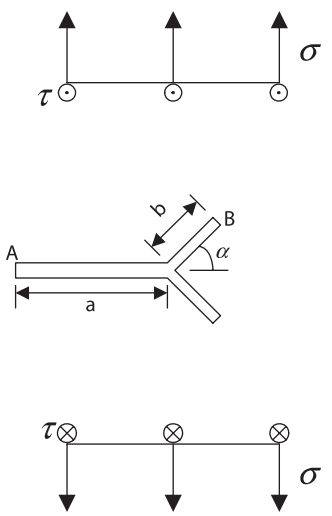

Figure 10. Branched crack under a far-field tensile stress σ and out-of-plane shear stress τ.

Example 4 (*Anisotropic rectangular plate under a uniform tension*)
In order to evaluate the influence of material anisotropy on the SIFs, consider an anisotropic rectangular plate of width $2w$ and height $2h$ with a central crack inclined 45° to the x-axis, as

DOI: 10.1002/nag

Table IV. Normalized SIFs for a branched crack in an infinite domain.

$b/a=0.6$	$K_{\mathrm{I}}^{A}/\sigma\sqrt{\pi a}$	$K_{\mathrm{I}}^{B}/\sigma\sqrt{\pi a}$	$K_{\mathrm{II}}^{B}/\sigma\sqrt{\pi a}$
This study	1.027	0.496	0.484
Murakami [47]	1.029	0.497	0.485
Ammons and Vable [46]	1.027	0.496	0.484

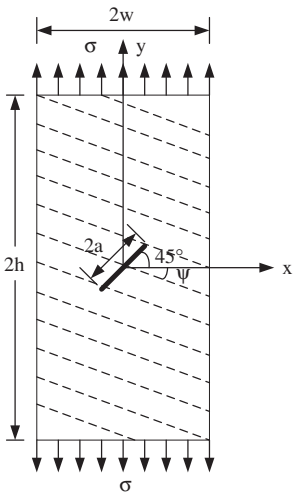

Figure 11. An anisotropic rectangular plate with a central crack inclined 45° under uniform tensile stress σ.

Table V. Normalized SIFs for a central slant in anisotropic rectangular plate subjected to a uniform tension ($\beta=45^{\circ}, a/R=0.5$).

	Gandhi [48]		Sollero and Aliabadi [17]		Chen *et al.* [26]		This study	
ψ (deg.)	$K_{\mathrm{I}}/\sigma\sqrt{\pi a}$	$K_{\mathrm{II}}/\sigma\sqrt{\pi a}$	$K_{\mathrm{I}}/\sigma\sqrt{\pi a}$	$K_{\mathrm{II}}/\sigma\sqrt{\pi a}$	$K_{\mathrm{I}}/\sigma\sqrt{\pi a}$	$K_{\mathrm{II}}/\sigma\sqrt{\pi a}$	$K_{\mathrm{I}}/\sigma\sqrt{\pi a}$	$K_{\mathrm{II}}/\sigma\sqrt{\pi a}$
0	0.522	0.507	0.517	0.506	0.519	0.504	0.524	0.514
45	0.515	0.505	0.513	0.502	0.516	0.505	0.518	0.513
90	0.513	0.509	0.515	0.510	0.537	0.532	0.533	0.527
105	0.517	0.510	0.518	0.512	0.507	0.502	0.540	0.528
120	0.524	0.512	0.526	0.513	0.520	0.508	0.541	0.526
135	0.532	0.511	0.535	0.514	0.532	0.511	0.536	0.522
180	0.522	0.507	0.517	0.506	0.519	0.504	0.524	0.514

shown in Figure 11. The plate is loaded with a uniform tensile stress in the y-direction. The ratios of crack length and of height to width are $a/W=0.2$ and $h/W=2.0$, respectively. The material is glass-epoxy with elastic properties $E=48.26\,\mathrm{GPa}$, $E'=17.24\,\mathrm{GPa}$, $v'=0.29$, and $G'=6.89\,\mathrm{GPa}$ [7]. The direction of the fibers is rotated from $\psi=0$ to 180°. The outer boundary and crack surface are discretized with 32 continuous and 10 discontinuous quadratic elements, respectively. Table V

DOI: 10.1002/nag

shows the results obtained by the proposed method as well as those by Sollero and Aliabadi [17], Gandhi [48], and Chen *et al*. [26]. Again, an excellent agreement is obtained.

4. MODELING CRACK PROPAGATION PATH

The proposed BEM formulation combined with the maximum circumferential stress criterion is developed to predict the angle of crack initiation and to simulate the path of crack propagation under mixed-mode loading. The crack propagation process in the cracked materials is numerically estimated by two-dimensional stress and displacement analysis. In order to understand the behavior of cracks under mixed-mode loading, the BEM program is applied.

4.1. Crack initiation

The proposed BEM formulation is also used to predict the initial growth of cracks in anisotropic materials. To examine the validity of our crack initiation prediction procedure, the tests of Erdogan and Sih [28] and Vallejo [34] are reproduced numerically with our BEM program.

Erdogan and Sih [28] conducted uniaxial tension test on isotropic Plexiglass sheets $229 \times 457 \times 4.8$ mm in size containing a 50.8 mm central crack. The crack inclination angle β between the crack plane and the tensile stress is varied. Figure 12 shows the variation of the crack initiation angle θ_0 with the crack angle β determined numerically and experimentally. A good agreement is found between the experimental results of Erdogan and Sih [28] and our numerical predictions.

Other verification is done using the experimental results of Vallejo [34]. The uniaxial compression tests were conducted on cracked prismatic specimens of kaolinite clay $76.2 \times 76.2 \times 25.4$ mm in size containing a central crack 24.9 mm in length by Vallejo [34]. Several tests are carried out by varying the crack angle β between the crack plane and the compressive stress. Figure 13 shows

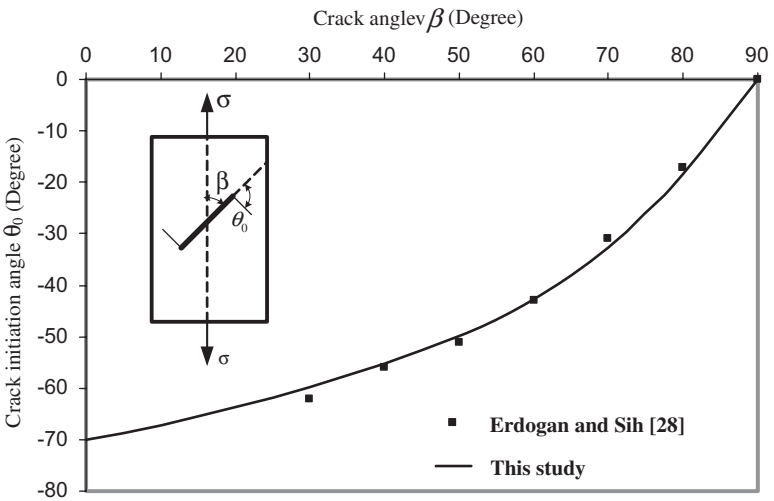

Figure 12. Variation of crack initiation angle θ_0 with the crack angle β. Plexiglass plate subjected to uniaxial tension.

DOI: 10.1002/nag

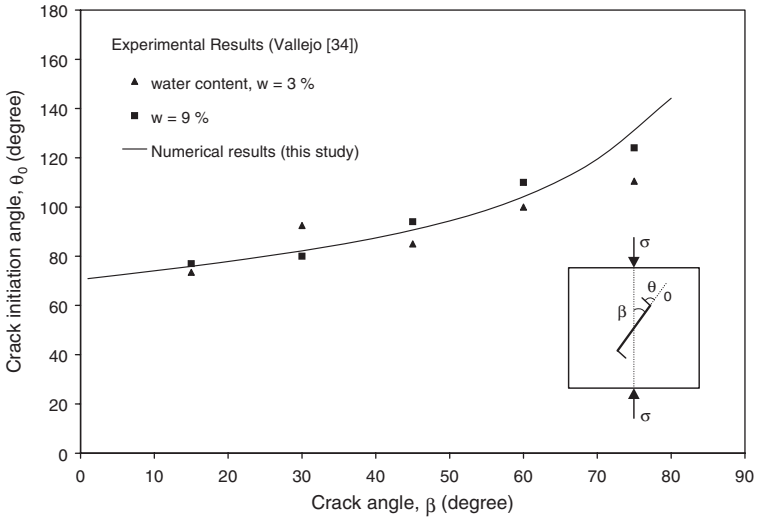

Figure 13. Variation of crack initiation angle θ_0 with the crack angle β. Prismatic sample of kaolinite clay subjected to uniaxial compression.

a comparison between the crack initiation angles measured experimentally and those predicted numerically. Again, a good agreement is found with the experimental results.

4.2. Crack propagation path

Two examples of the isotropic cracked plate under pure mode I and II loading and the anisotropic cracked Brazilian disc under mixed-mode I–II loading are carried out to investigate the validity of the current crack propagation modeling for the BEM formulation.

Example 1 (*Isotropic cracked plate under pure mode I and mode II loading*)
The behavior of an existing crack under pure mode I loading or pure mode II loading is studied for the application. The first problem, as shown in Figure 14(a), is a square plate with a horizontal edge crack subjected to uniaxial tension. The width of the square plate is w. The initial crack length, a, is equal to $w/3$. The no-crack boundary and crack surface are discretized with 55 continuous and 10 discontinuous quadratic elements, respectively. According to the experimental results from Erdogan and Sih [28], it is known that the crack propagation angle (θ) is zero when the crack inclination angle (β) is 90° with respect to the y-axis, which means the crack will propagate along the horizontal direction. Figure 15 shows the path of crack propagation under pure mode I loading. It is shown that the path of crack propagation is a horizontal line, which is in full agreement with the experimental results made by Erdogan and Sih [28].

With the same configuration and the discretization of the first problem, the second problem subjected to a pure mode II loading, as shown in Figure 14(b), is further studied. Figure 16 shows the path of crack propagation. It can be observed that the path of crack propagation is approximately perpendicular to the crack surface. The full propagation path is similar to the numerical results obtained by Poterla [12].

DOI: 10.1002/nag

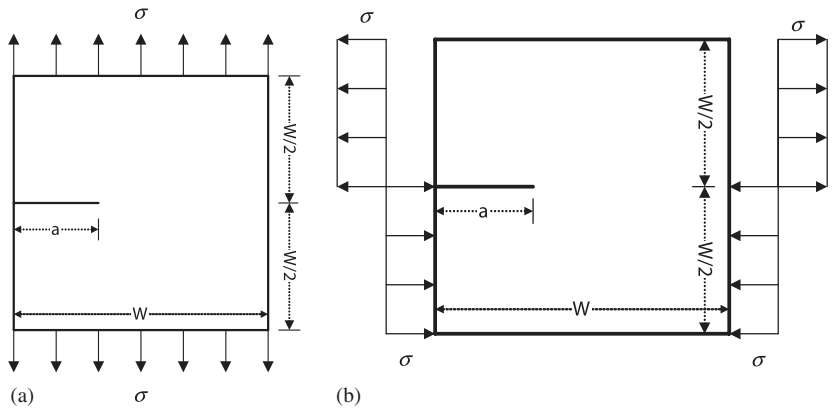

Figure 14. Square plate with a straight edge crack under pure mode I and mode II.

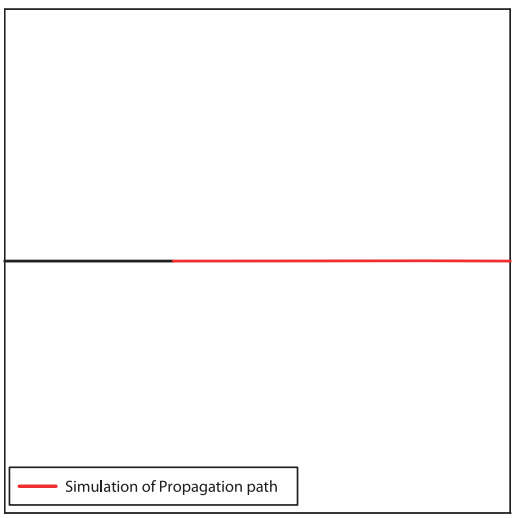

Figure 15. Crack propagation path and normalized SIFs of the cracked plate initially under pure mode I loading.

Example 2 (*Anisotropic cracked Brazilian disc specimens under mixed-mode I–II loading*)
To demonstrate the proposed BEM procedure when predicting crack propagation in the anisotropic materials under mixed-mode I–II loading, the propagation path in a CSTBD specimen is numerically predicted and compared with the actual laboratory observations. In these experiments, a crack initially inclined with respect to the applied stress is allowed to grow under concentrated diametrical loading. The Brazilian tests on CSTBD specimens with a diameter of 7.4 cm, a thickness of 1 cm, and a crack length of 2.2 cm are conducted to observe the actual propagation paths and are compared with the numerical predictions. Details of the experimental procedure can be found in the paper by Ke *et al*. [49]. The five elastic constants of anisotropic marble are $E = 78.302$ GPa,

DOI: 10.1002/nag

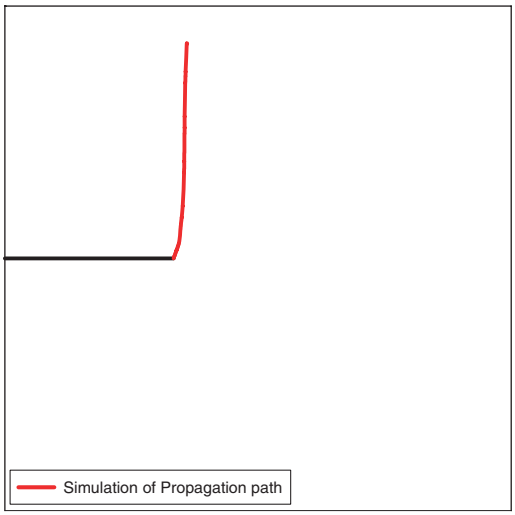

Figure 16. Crack propagation path and normalized SIFs of the cracked plate initially under pure mode II loading.

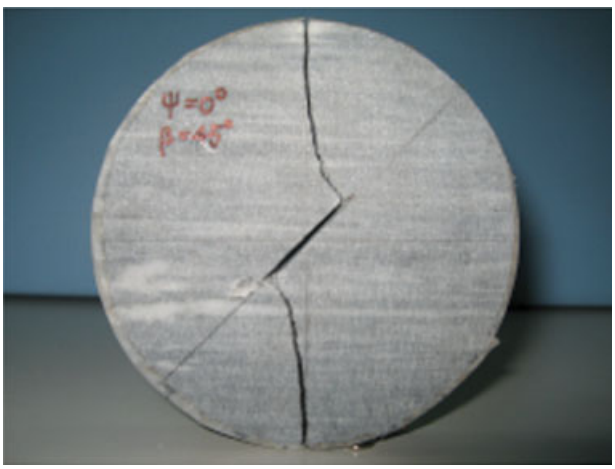

Figure 17. Photograph of specimen AM-4 after failure ($\psi=0°$ and $\beta=45°$).

$E'=67.681\,\text{GPa}$, $v=0.267$, $v'=0.185$, $G=30.735\,\text{GPa}$, and $G'=25.336\,\text{GPa}$, respectively. The ratios of E/E' and E/G' are 1.156 and 3.091, respectively. Since the value of $E/E'=1.156$, this marble can be classified as a slightly anisotropic rock.

Four specimens with the material inclination angle $\psi=45°$, defined as the AM-4, CM-4, DM-4, and EM-4, have crack angles $\beta=0°, 30°, 45°$, and $60°$ respectively. After Brazilian tests with

DOI: 10.1002/nag

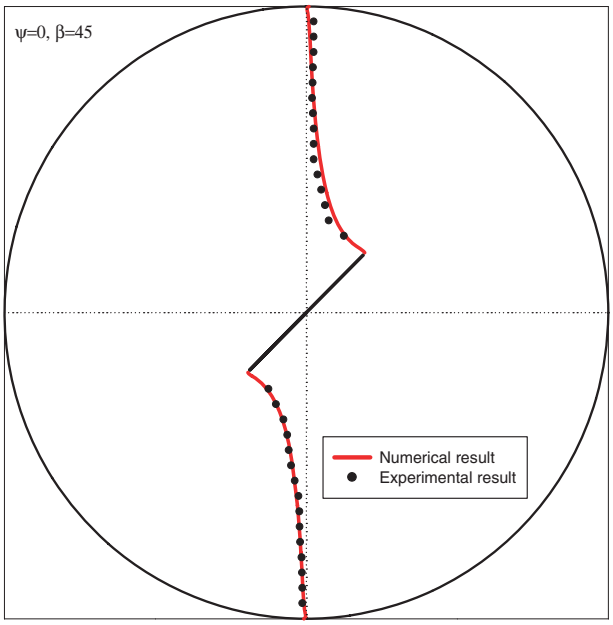

Figure 18. Propagation of a crack at the center of a CSTBD specimen with $\psi = 0°$ and $\beta = 45°$. Comparison between experimental observations and numerical predictions for specimen AM-4.

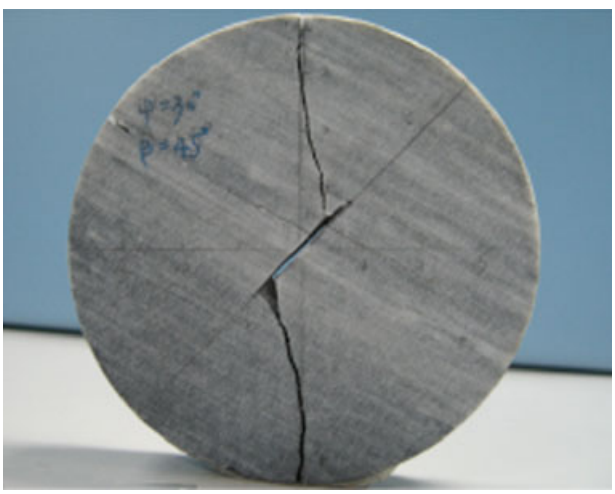

Figure 19. Photograph of specimen CM-4 after failure ($\psi = 30°$ and $\beta = 45°$).

cracked specimens, the paths of crack propagation for AM-4, CM-4, DM-4, and EM-4 are shown in Figures 17, 19, 21, and 23, respectively. It can be observed that the crack propagates nearly perpendicular to the crack surface in the initial stage and then rapidly approaches toward the

DOI: 10.1002/nag

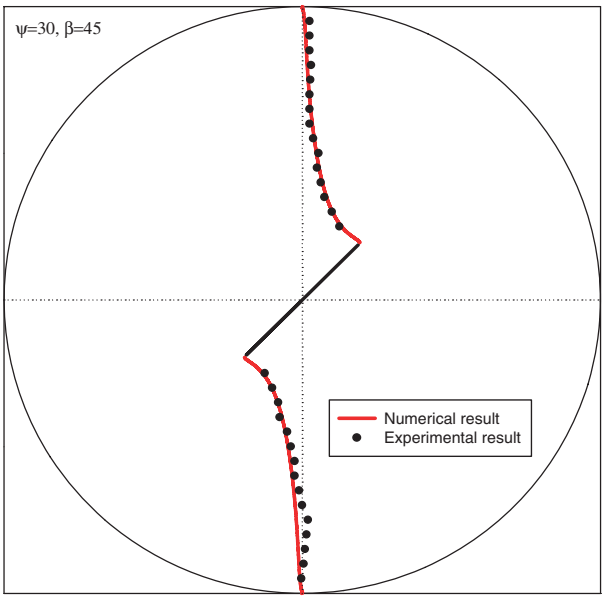

Figure 20. Propagation of a crack at the center of a CSTBD specimen with $\psi = 30°$ and $\beta = 45°$. Comparison between experimental observations and numerical predictions for specimen CM-4.

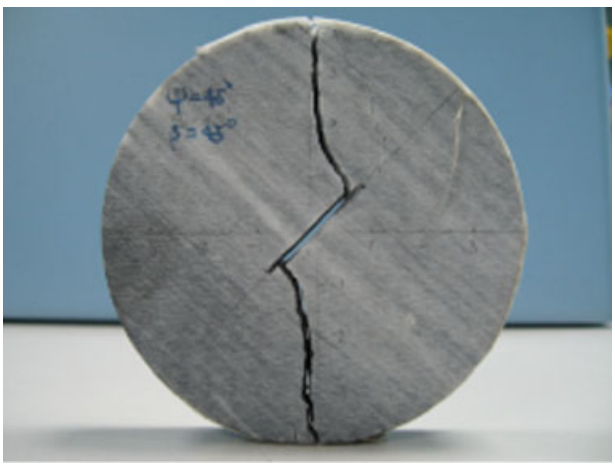

Figure 21. Photograph of specimen DM-4 after failure ($\psi = 45°$ and $\beta = 45°$).

loading point. The proposed BEM procedure is also used to simulate crack propagation in the CSTBD specimens. The outer boundary and crack surface are discretized with 28 continuous and 20 discontinuous quadratic elements, respectively. Figures 18, 20, 22, and 24 are the comparisons

DOI: 10.1002/nag

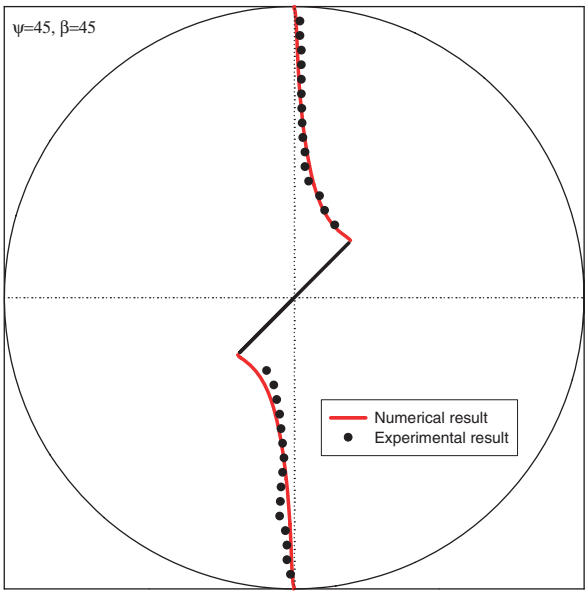

Figure 22. Propagation of a crack at the center of a CSTBD specimen with $\psi = 45°$ and $\beta = 45°$. Comparison between experimental observations and numerical predictions for specimen DM-4.

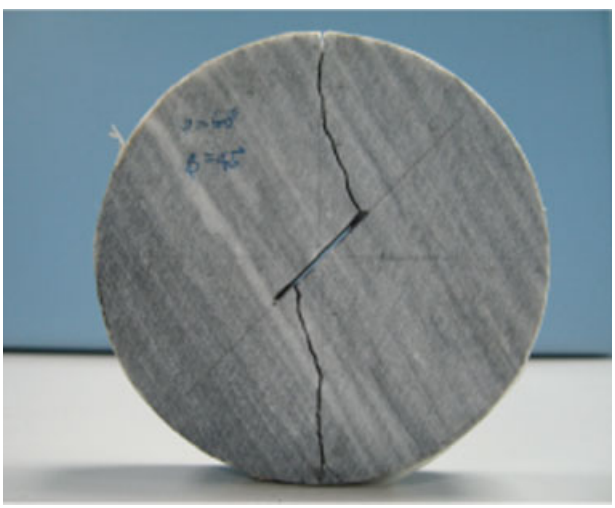

Figure 23. Photograph of specimen EM-4 after failure ($\psi = 60°$ and $\beta = 45°$).

of crack propagation paths between experimental observations and numerical predictions in AM4, CM-4, DM-4, and EM-4, respectively. Again, the proposed BEM procedure accurately simulates the crack propagation in these anisotropic specimens. According to the simulations of foregoing

DOI: 10.1002/nag

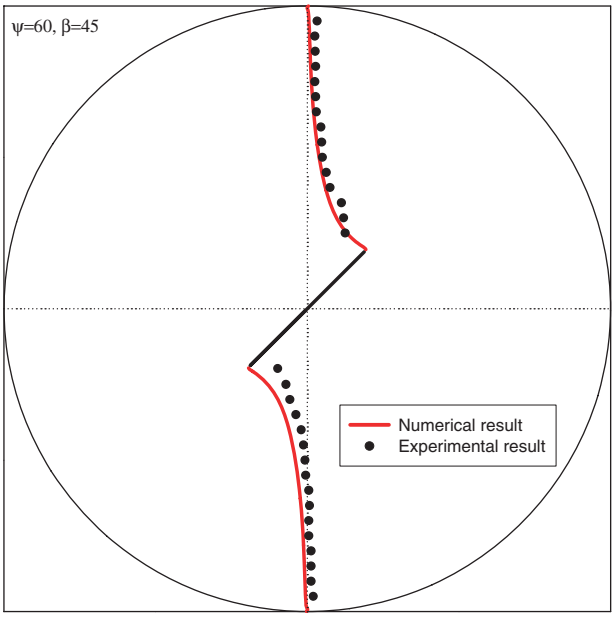

Figure 24. Propagation of a crack at the center of a CSTBD specimen with $\psi = 60°$ and $\beta = 45°$. Comparison between experimental observations and numerical predictions for specimen EM-4.

examples, it can be concluded that the proposed BEM is capable of predicting the crack propagation in anisotropic rocks.

5. CONCLUSIONS

In this paper, a formulation of the BEM, based on the relative displacements near the crack tip, is utilized to determine the mixed-mode SIFs of anisotropic rocks. The BEM formulation is such that the displacement integral equation is collocated on the outer boundary only and the traction integral equation on one side of the crack surface only. The extrapolation method can be used to determine the mixed-mode SIFs based on the relative displacements near the crack tip. Numerical examples for the determination of the mixed-mode SIFs for a CSTBD specimen are presented for isotropic and anisotropic media. The numerical results obtained by the proposed method are in good agreement with those reported by previously published results. In addition, the SIFs for a curved crack and branched crack under far-field tensile stress and anti-plane shear stress are also determined by the proposed BEM formulation. The numerical results obtained by this study are in agreement with those reported by previously published results.

This paper presents the development of BEM procedure based on the maximum circumferential stress criterion for predicting the crack initiation directions and propagation paths in isotropic and anisotropic materials under mixed-mode loading. Good agreements are found between crack initiation and propagation predicted with the BEM and experimental observations reported by previous researchers of isotropic materials. Numerical simulations of crack initiation and propagation in CSTBD specimens of the anisotropic rock are also found to compare well with experimental results.

DOI: 10.1002/nag

NOMENCLATURE

β	the crack inclination angle (deg.)
ψ	the material orientation angle (deg.)
a	the half crack length
CSTBD	the cracked straight through Brazilian disc
D	the diameter of Brazilian disc
E	Young's modulus
SIF(s)	the Stress Intensity Factor(s)
K_{I}	the mode I SIF ($\mathrm{MPa\,m^{1/2}}$)
K_{II}	the mode II SIF ($\mathrm{MPa\,m^{1/2}}$)
F_{I}	the normalized mode I SIF
F_{II}	the normalized mode II SIF
R	the radius of the Brazilian disc
t	the thickness of the Brazilian disc
W_{f}	the failure load

REFERENCES

1. Griffith AA. The phenomena of rupture and flow in solids. *Philosophical Transactions of the Royal Society* 1921; **A221**:163–198.
2. Irwin GR. Analysis of stresses and strains near the end of a crack. *Journal of Applied Mechanics* 1957; **24**:361–364.
3. Denda M. Mixed mode I, II and III analysis of multiple cracks in plane anisotropic solids by the BEM: a dislocation and point force approach. *Engineering Analysis with Boundary Elements* 2001; **25**:267–278.
4. Snyder MD, Cruse TA. Boundary-integral equation analysis of cracked anisotropic plates. *International Journal of Fracture* 1975; **11**:315–328.
5. Dumir PC, Mehta AK. Boundary element solution for elastic orthotropic half-plane problems. *Computers and Structures* 1987; **26**(3):431–438.
6. Blandford GE, Ingraffea AR, Liggett JA. Two-dimensional stress intensity factor computations using the boundary element method. *International Journal for Numerical Methods in Engineering* 1981; **17**:387–404.
7. Sollero P, Aliabadi MH. Fracture mechanics analysis of anisotropic plates by the boundary element method. *International Journal of Fracture* 1993; **64**:269–284.
8. Sollero P, Aliabadi MH, Rooke DP. Anisotropic analysis of cracks emanating from circular holes in composite laminates using the boundary element method. *Engineering Fracture Mechanics* 1994; **49**:213–224.
9. Crouch SL, Starfield AM. *Boundary Element Methods in Solid Mechanics*. George Allen and Unwin: London, 1983.
10. Shen B, Stephansson O. Modification the G-criterion for crack propagation subjected to compression. *Engineering Fracture Mechanics* 1994; **47**(2):177–189.
11. Scavia C. A method for the study of crack propagation in rock structures. *Geotechnique* 1995; **45**(3):447–463.
12. Portela A. *Dual Boundary Element Analysis of Crack Growth*. Computational Mechanics: U.K., U.S.A., 1993.
13. Hong HK, Chen JT. Derivations of integral equations of elasticity. *Journal of Engineering Mechanics* 1988; **114**:1028–1044.
14. Gary LJ, Martha LF, Ingraffea AR. Hypersingular integrals in boundary element fracture analysis. *International Journal for Numerical Methods in Engineering* 1990; **29**:1135–1158.
15. Portela A, Aliabadi MH, Rooke DP. The dual boundary element method: effective implementation for crack problems. *International Journal for Numerical Methods in Engineering* 1992; **33**:1269–1287.
16. Portela A, Aliabadi MH, Rooke DP. Dual boundary element incremental analysis of crack growth. *Composite Structures* 1993; **46**(2):237–284.
17. Sollero P, Aliabadi MH. Anisotropic analysis of cracks in composite laminates using the dual boundary element method. *Composite Structures* 1995; **31**:229–233.

DOI: 10.1002/nag

18. Sollero P, Aliabadi MH. Dual boundary element analysis of anisotropic crack problems. *Boundary Elements XVII*. Computational Mechanics: Southampton, 1995; 267–278.
19. Pan E, Amadei B. Fracture mechanics analysis of cracked 2-D anisotropic media with a new formulation of the boundary element method. *International Journal of Fracture* 1996; **77**:161–174.
20. Pan E. A general boundary element analysis of 2-D linear elastic fracture mechanics. *International Journal of Fracture* 1997; **88**:41–59.
21. Aliabadi MH. A new generation of boundary element methods in fracture mechanics. *International Journal of Fracture* 1997; **86**:91–125.
22. Chen JT, Hong HK. Review of dual boundary element methods with emphasis on hypersingular integrals and divergent series. *Transactions of the ASME*, *Applied Mechanics Review* 1999; **52**(1):17–33.
23. Cisilino AP, Aliabadi MH. Three-dimensional boundary element analysis of fatigue crack growth in linear and non-linear fracture problems. *Engineering Fracture Mechanics* 1999; **63**:713–733.
24. Wilde AJ, Aliabadi MH. Boundary element analysis of geomechanical fracture. *International Journal for Numerical and Analytical Methods in Geomechanics* 1999; **23**:1195–1214.
25. Jing L. A review of techniques, advances and outstanding issues in numerical modelling for rock mechanics and rock engineering. *International Journal of Rock Mechanics and Mining Sciences* 2003; **40**:283–353.
26. Chen CS, Pan E, Amadei B. Fracture mechanics analysis of cracked discs of anisotropic rock using the boundary element method. *International Journal of Rock Mechanics and Mining Sciences* 1998; **35**(2):195–218.
27. Cruse TA. *Surface Cracks*: *Physical Problems and Computational Solutions*, Swedlow JL (ed.). ASME: New York, 1972.
28. Erdogan F, Sih GC. On the crack extension in plates under loading and transverse shear. *Transactions of the ASME*, *Journal of Basic Engineering* 1963; **85**:519–527.
29. Whittaker BN, Singh RN, Sun G. *Rock Fracture Mechanics Principles*, *Design and Applications*. Elsevier Publishers: Netherlands, 1992.
30. Boone TJ, Wawezynek PA, Ingraffea AR. Finite element modeling of fracture propagation in orthotropic materials. *Engineering Fracture Mechanics* 1987; **26**(2):185–201.
31. Ayatollahi MR, Aliha MRM. On determination of mode II fracture toughness using semi-circular bend specimen. *International Journal of Solids and Structures* 2006; **43**:5217–5227.
32. Woo CW, Ling LH. On angled crack initiation under biaxial loading. *Journal of Strain Analysis* 1984; **19**(1):51–59.
33. Richard HA. Examination of brittle fracture criteria for overlapping mode I and mode II loading applied to cracks. In *Application of Fracture Mechanics to Materials and Structures*, Sih GC *et al.* (eds). Martinus Nijhoff Publication: Netherlands, 1984; 309–316.
34. Vallejo LE. The brittle and ductile behavior of a material containing a crack under mixed-mode loading. *Proceedings of the 28th U.S. Symposium on Rock Mechanics*, University of Arizona, Tucson, 1987.
35. Bouchard PO, Bay F, Chastel Y, Tovena I. Crack propagation modeling using an advanced remeshing technique. *Computer Methods in Applied Mechanics and Engineering* 2000; **189**:723–742.
36. Ku CY. Modeling of jointed rock masses based on the numerical manifold method. *Ph.D. Dissertation*, Department of Civil and Environmental Engineering, University of Pittsburgh, 2001.
37. Al-Shayea NA. Crack propagation trajectories for rocks under mixed mode I–II fracture. *Engineering Geology* 2005; **81**:84–97.
38. Lekhnitskii SG. *Theory of Elasticity of an Anisotropic Elastic Body*. Translated by Fern P. Holden-Day Inc.: San Francisco, 1981.
39. Amadei B. *Rock Anisotropy and the Theory of Stress Measurements*. Springer: New York, 1987.
40. Sih GC, Paris PC, Irwin GR. On cracks in rectilinearly anisotropic bodies. *International Journal of Fracture* 1965; **3**:189–203.
41. Suo Z. Singularities, interfaces, cracks in dissimilar anisotropic media. *Proceedings of the Royal Society* 1990; **A427**:331–358.
42. Cerrolaza M, Alarcon E. A bi-cubic transformation for the numerical evaluation of the Cauchy principal value integrals in boundary methods. *International Journal for Numerical Methods in Engineering* 1989; **28**:987–999.
43. Sih GC. *Mechanics of Fracture Initiation and Propagation*: *Surface and Volume Energy Density Applied as Failure Criterion*. Kluwer Academic: Boston, 1991.
44. Atkinson C, Smelser RE, Sanchez J. Combined mode fracture via the cracked Brazilian disk test. *International Journal of Fracture* 1982; **18**:279–291.
45. Tada H, Paris PC, Irwin GR. *The Stress Analysis of Cracks Handbook* (2nd edn). Paris Productions Incorporated: Missouri, 1985.

DOI: 10.1002/nag

46. Ammons BA, Vable M. Boundary element analysis of cracks. *International Journal of Solids and Structures* 1996; **33**:1853–1865.
47. Murakami Y. *Stress Intensity Factors Handbook*. Pergamin Press: Oxford, 1987.
48. Gandhi KR. Analysis of inclined crack centrally placed in an orthotropic rectangular plate. *Journal of Strain Analysis* 1972; **7**(3):157–162.
49. Ke CC, Chen CS, Tu CH. Determination of fracture toughness of anisotropic rocks by boundary element method. *Rock Mechanics and Rock Engineering* 2008; **41**(4):509–538.

DOI: 10.1002/nag